Hole doping and pressure effects on the II-II-V-based diluted magnetic semiconductor $(Ba_{1-x}K_{x})(Zn_{1-y}Mn_{y})_{2}As_{2}$

F. Sun, G. Q. Zhao, C. A. Escanhoela, Jr., B. J. Chen, R. H. Kou, Y. G. Wang, Y. M. Xiao, P. Chow, H. K. Mao, D. Haskel, W. G. Yang, and C. Q. Jin

Phys. Rev. B **95**, 094412 — Published 13 March 2017

DOI: 10.1103/PhysRevB.95.094412

Hole-doping and pressure effects on the II-II-V based diluted magnetic semiconductor $(Ba_{1-x}K_x)(Zn_{1-y}Mn_y)_2As_2$

F. Sun[1,2], G. Q. Zhao[1], C. A. Escanhoela Jr.[3], B. J. Chen[1], R. H. Kou[2], Y. G. Wang[4], Y. M. Xiao[5], P. Chow[5], H. K. Mao[4,6], D. Haskel[2,*],W. G. Yang[4,6,*], C. Q. Jin[1,7,*]

[1]*Beijing National Laboratory for Condensed Matter Physics and Institute of Physics, Chinese Academy of Sciences, Beijing 100190,China.*

[2]*Advanced Photon Source, Argonne National Laboratory, Argonne, Illinois 60439, USA.*

[3] *Brazilian Synchrotron Light Laboratory (LNLS), Campinas, SP 13083-970, Brazil.*

[4]*High Pressure Synergetic Consortium (HPSynC), Geophysical Laboratory, Carnegie Institution of Washington, Argonne, Illinois 60439, USA.*

[5]*HPCAT, Carnegie Institution of Washington, Argonne, Illinois 60439, USA.*

[6]*Center for High Pressure Science & Technology Advanced Research (HPSTAR), Shanghai, 201203, China.*

[7]*Collaborative Innovation Center of Quantum Matter, Beijing, China.*

***Corresponding authors:** haskel@aps.anl.gov; yangwg@hpstar.ac.cn; jin@iphy.ac.cn

Abstract

We investigate doping- and pressure-induced changes in the electronic state of Mn 3*d* and As 4*p* orbitals in II-II-V based diluted magnetic semiconductor $(Ba_{1-x},K_x)(Zn_{1-y},Mn_y)_2As_2$ to shed light into the mechanism of indirect exchange interactions leading to high ferromagnetic ordering temperature (*T*c = 230 K in optimally doped samples). A suite of x-ray spectroscopy experiments (emission, absorption and dichroism) show that the emergence, and further enhancement of ferromagnetic interactions with increased hole doping into the As 4*p* band is accompanied by a decrease in local 3*d* spin density at Mn sites. This is a result of increasing Mn 3*d* - As 4*p* hybridization with hole doping which enhances indirect exchange interactions between Mn dopants and gives rise to induced magnetic polarization in As 4*p* states. On the contrary, application of pressure suppresses exchange interactions. While Mn Kβ emission spectra show a weak response of 3*d* state to pressure, clear As 4*p* band broadening (hole delocalization) is observed under pressure ultimately leading to loss of ferromagnetism concomitant with a semiconductor to metal transition. The pressure response of As 4*p* and Mn 3*d* states is intimately connected with the evolution of the As-As interlayer distance and the geometry of the $MnAs_4$ tetrahedral units, which we probed with X-ray diffraction. Our results indicate that hole doping increases the degree of covalency between the anion (As) *p* states and cation (Mn) *d* states in the $MnAs_4$ tetrahedron, a crucial ingredient to promote indirect exchange interactions between Mn dopants and high *T*c ferromagnetism. The instability of ferromagnetism and semiconducting state against pressure is mainly dictated by delocalization of anion *p* states.

Introduction

Since the discovery of carrier-mediated ferromagnetism in Mn-doped InAs and GaAs compounds, diluted magnetic semiconductors (DMS) have received extensive attention due to their potential for manipulation of electron spin as a foundation of semiconductor spintronics [1-5]. Much progress has been made in the control of the exchange interactions, in which the magnetic phase can be turned on and off by applying electric field, light irradiation, or external pressure [6]. However, a microscopic understanding of the physical properties of DMS is still limited, e.g., the mechanism leading to magnetic ordering of dopants remains strongly debated [5, 7]. Similarly, applications of high-*T*c DMS in devices are yet to be realized. In the Mn-doped III-V semiconductors, substitution of trivalent cation Ga for Mn simultaneously introduces an acceptor and a source of magnetic moments. This dual role of Mn complicates theoretical understanding. Recently, Mn-doped II-II-V based semiconductor $Ba(Zn,Mn)_2As_2$ was shown to become a high *T*c

ferromagnet upon hole doping. Holes doped into the ZnAs layer through substitution of K^+ ions into the Ba^{2+} sites mediate the interaction between magnetic ions and induce ferromagnetism with *T*c as high as 180 K in $(Ba_{1-x}K_x)(Zn_{0.9}Mn_{0.1})_2As_2$ with $x = 0.3$ [8]. Improved synthesis techniques have since enhanced the ferromagnetic ordering temperature to 230 K [9], approaching the long sought DMS at room temperature [10].

This new bulk DMS material is isostructural to the ferropnictide "122" RFe_2As_2 (R = Ba, Sr, Ca) class of superconductors [11] where [(Zn/Mn)As] layers alternate with [Ba/K] layers. The strategy of transforming the non-magnetic phase $Ba(Zn,Mn)_2As_2$ into a ferromagnetic phase is analogous to the recipe used to induce superconductivity in iron-based superconductors, i.e. through doping of the [Ba/K] charge reservoir layers. In previous work [12], studies using the XMCD technique showed that the long-range magnetic order in $(Ba_{1-x}K_x)(Zn_{1-y}Mn_y)_2As_2$ is mediated by the *p* states of As through As 4*p* - Mn 3*d* hybridization, and that the As *K*-edge XMCD intensity (polarization of doped hole carriers) is strongly connected with the magnetic ordering of the bulk sample. These results support recent theoretical calculations [13] on Mn-doped II-II-V semiconductor which predict that the mediating states are primarily derived from As 4*p* valence band states, and that *p-d* hybridization between Mn 3*d* and As 4*p* orbitals plays an important role in the exchange coupling between localized spins and itinerant holes. However, the evolution of Mn 3*d* and As 4*p* states (and their hybridization) with hole doping, and its impact on exchange interactions leading to high *T*c ferromagnetic ordering temperatures, are still not fully understood and await further experimental and theoretical investigations. Probing the electronic states of localized spins (Mn 3*d*) and mediating hole carriers (As 4*p*) is necessary to test theoretical band structure models which have recently been employed to interpret experimental findings [4].

In this paper, we have performed element- and orbital-resolved X-ray spectroscopy measurements on $Ba(Zn,Mn)_2As_2$ DMS at ambient- and high-pressures. These include X-ray emission spectroscopy (XES) and X-ray absorption spectroscopy (XAS) measurements at the Mn *K*-edge, and X-ray magnetic circular dichroism (XMCD) measurements at the As *K*-edge. XAS probes the unoccupied electronic states, and can also yield valence information from the chemical shift of the absorption edge [14]. Complementary to XAS techniques, *K*-shell XES provides access to the occupied density of states and can provide information on the magnitude of local moments in 3*d* metals [15, 16]. XMCD, on the other hand, which measures the difference in absorption of a magnetized sample for opposite helicity of circularly polarized X-rays, is a probe of ferromagnetic order [17] and allows studying the spin polarization of As 4*p* charge carriers. These information, key to understanding the indirect exchange interactions in DMS systems, is hardly accessible with macroscopic probes such as superconducting quantum interference device (SQUID) magnetometry which is dominated by the response of Mn spins. The combination of XAS, XES and XMCD probes allows us to investigate the electronic properties of $Ba(Zn,Mn)_2As_2$ DMS at ambient- and high- pressure conditions with exquisite selectivity. Since electronic structure is intimately connected to crystal structure we also probed the evolution of crystal structure under pressure with X-ray diffraction (XRD) measurements, providing further insight into the microscopic origin of the pressure-driven semiconducting/ferromagnetic to metallic/paramagnetic transition.

Experimental details

Polycrystalline samples of $(Ba_{1-x}K_x)(Zn_{1-y}Mn_y)_2As_2$ were synthesized using the arc-melting solid-state reaction method [8, 18]. The series of studied samples was labeled G*m* (*m* = 0, 1, 2, 3, 4). Compounds with different K (hole) doping level *x* (*x* = 0, 0.15, 0.25) at fixed Mn (spin) concentration y = 0.15 were used to study the hole-doping effect. These samples are labeled as G0 (x = 0, y = 0.15), G1 (x = 0.15, y = 0.15) and G2 (x = 0.25, y = 0.15). For unraveling the effect of pressure, hole under-doped G1 (x = 0.15, y = 0.15) and optimally hole doped G3 (*x* = 0.25, *y* = 0.05) compounds were used. Since samples are isostructural for all *x*, *y* values studied here, the G4 (*x* = 0.20, *y* = 0.05) sample was used in XRD measurements as representative to understand the structural response to pressure.

The non-resonant Mn Kβ XES experiments were performed at beamline 16 ID-D of the Advanced Photon Source (APS) at Argonne National Laboratory. The ambient- and high- pressure XES data were obtained in separate experiments using incident energies of 16.1 KeV and 11.3 KeV respectively. The energy of emitted photons was analyzed using a four-inch spherically bent Si (422) crystal which was arranged with the sample and detector in a vertical Rowland geometry (R ~ 1 m). The average of the full width at half maximum (FWHM) of the elastically scattered photons was about 1 eV. The high-pressure XES data was collected using a Mao-Bell Symmetric Diamond Anvil Cell (DAC) with 300 microns culet anvils. A beryllium gasket, pre-indented and further drilled into a sample chamber with a diameter of 120 microns, was used to allow efficient detection of the low-energy Kβ X-ray emission. Ruby ball was placed near the sample chamber edge and used as pressure marker. For the temperature dependent measurements at ambient pressure, a pelletized sample was mounted on a copper holder with grease and loaded into a He-flow cryostat with an automatic temperature control system. The Mn *K*-edge XAS experiments at ambient condition were carried out at beamline 20 BM-B of APS, using a Si (111) monochromator. Finely grounded powder samples were mixed with Boron nitride powder and pelletized, with sample thickness optimized for transmission measurements. Energy calibration was monitored for each spectrum using simultaneous measurements on a reference manganese metal foil.

The As *K*-edge XMCD experiments were performed at beamline 4 ID-D of APS. Polycrystalline samples were grounded into fine powder before the experiment. Pressure experiments used a membrane-driven, CuBe DAC placed inside the bore of a cryogenic superconducting magnet and cooled with He vapor. To avoid sizable pressure increase on cooling, a large culet size of 1 mm was used for the measurements on the G1 sample below 5 GPa. Data above 5 GPa was obtained with 300 microns culets. Powder sample was mixed with silicon oil as pressure-transmitting medium before loading into the DACs. Stainless steel was chosen as the gasket and ruby ball was placed near the edge of the sample chamber for in-situ pressure calibration. The high pressure XMCD data on the G3 compound is taken from our previous work in Ref. 12. For ambient pressure XMCD measurements at low temperature, samples were mounted on tapes and stacked layer by layer to obtain the desired sample thickness. XMCD measurements were carried out in helicity-switching mode (13.1 Hz) using phase retarding optics, and the modulation in the X-ray absorption detected with a lock-in amplifier. Measurements were carried out for magnetic fields along and opposite X-ray propagation direction to remove artifacts of non-magnetic origin. The high-pressure powder XRD measurements were done at room temperature at beamline 16 BM-D of APS, using a Mao-Bell symmetric cell with 300 μm culets. The rhenium gasket was pre-indented to 40 μm and a sample chamber 170 μm in diameter drilled in the center of the indentation. Neon gas was used as pressure medium, resulting in a reduction of sample chamber diameter to 130 μm. Ruby balls were placed around the sample to monitor the pressure. The X-ray wavelength was 0.4246 Å and XRD patterns were collected with a MAR 3450 image plate detector.

Results and discussion

The evolution of lattice parameters and resistivity as a function of hole doping level x in polycrystalline $(Ba_{1-x}K_x)(Zn_{0.85}Mn_{0.15})_2As_2$ samples [G0 (x = 0), G1(x = 0.15) and G2 (x = 0.25)], together with the magnetic ordering temperature Tc of G1 and G2 samples, are shown in Figure 1 (a) and Figure 1 (b). Figure 1 (c) displays the DC magnetization data measured in G0, G1 and G2 samples. A clear upturn is observed around 90 K and 230 K for the G1 and G2 samples, respectively, indicating the development of ferromagnetic order in these compounds. In contrast, the sample G0 with no potassium content shows no such ferromagnetic upturn. Muon spin relaxation (MuSR) measurements on polycrystalline samples demonstrate that the long-range ferromagnetic ordering is an intrinsic bulk property [8]. Figure 2(a) shows the Mn Kβ XES spectra measured at room temperature for G0, G1 and G2 samples. The Kβ XES is mainly composed of the strong K$\beta_{1,3}$ line and a less intense Kβ' satellite line at a lower emission energy. The 3*p*3*d* exchange interaction model [19, 20] has satisfactorily explained this split structure. K$\beta_{1,3}$ line peak is slightly asymmetric with a weaker shoulder on the low energy side. This structure is known as the Kβ_x line,

and arises from a final state where an electron in the 3*d* valence band flips its spin [19]. The energy difference between the K β' satellite and the main K $\beta_{1,3}$ line, $\Delta E'$ has been shown to be a reliable parameter for spectral analysis [15, 21]. XES spectra are normalized by their area and then aligned with the main peak of the G0 spectrum [22, 23]. The split energy $\Delta E'$ decreases with increasing carrier doping level x as shown in the inset of Figure 2(a), all the while the K β' peak intensity decreases. This implies that the Mn local spin moment has decreased with carrier doping, which could arise as a result of a change in electron density (degree of localization), a change in the number of unpaired 3*d* electrons localized on the metal ion [15, 24], or both. In the present case, where Mn is always in a high-spin configuration, the change in the Mn spin state simultaneously correlates with the change in the net charge and the effective spin on the Mn [19, 25]. In order to examine if the change of local spin state is due to a valence state change of Mn, we conducted XAS measurements at the Mn *K*-edge in $(Ba_{1-x}K_x)(Zn_{0.85}Mn_{0.15})_2As_2$. The XAS data analysis followed standard methods using the ATHENA software package [26]. Figure 2(b) shows XAS spectra at the Mn *K*-edge for the metallic manganese and G0, G1, G2 compounds at room temperature and ambient pressure. Clearly the local environment of the Mn dopants is not the same as that in Mn metal ruling out precipitation of Mn into small clusters. The valence state of Mn atoms does not change with varying x (hole doping). The degree of covalency induced by ligand field, more specifically hole-doping tuned degree of *p-d* orbital hybridization within $MnAs_4$ units, accounts for the variation of $\Delta E'$ (effective spin). The dependence of $\Delta E'$ on hole-doping is displayed in the inset of Figure 2(a). It decreases when *T*c increases (*T*c values shown next to compound labels) and indicates that *p-d* hybridization and related reduction in local spin density at Mn sites promotes magnetic coupling between Mn dopants in the measured samples.

The As *K*-edge XMCD spectra for G0, G1 and G2 compounds, measured at a base temperature of 2 K and external magnetic field of 4 T, are shown in Fig. 2(c). G1 and G2 compounds show robust XMCD signal. The dichroic signal consists of a single peak which is located at the low energy side of the As *K* absorption edge. By applying the *s* (l = 0) core level orbital magnetization sum rule [27-29], we obtained the orbital magnetic moment per As ion for different hole doping levels, as shown in the inset of Figure 2(c). Its magnitude is strongly sample dependent: samples with higher ferromagnetic *T*c exhibit larger XMCD signals, which is consistent with our previous observation that As *K*-edge XMCD is representative of the bulk magnetization [12]. The larger XMCD signal for the x = 0.25 compound is related to a stronger 4*p*-3*d* hybridization resulting in larger induced magnetic polarization at As sites. The absence of XMCD signal in the undoped x = 0 compound supports the conclusion that the As 4*p* band does not become magnetically polarized unless holes are doped into this band and order of Mn moments emerges.

The XES, XAS and XMCD measurements, taken together, indicate that upon hole doping the effective local Mn 3*d* moments are gradually reduced and As 4*p* states become magnetically polarized in the opposite direction [12], consistent with *p-d* hybridization. This implies that hole-doping drives an electron redistribution within $MnAs_4$ tetrahedra without changing the valence state of Mn atoms. This, in turn, enhances the indirect exchange interaction between diluted magnetic atoms through *p-d* hybridization.

It is known that a high-spin to low-spin transition can be triggered by a redistribution of the 3*d* electrons within the t_{2g} and e_g orbitals with variation in temperature [23]. In order to explore how the diluted local spin state evolves when a sample is driven into the ferromagnetic ordering phase with temperature, we have conducted temperature-dependent Mn K β XES measurements on $(Ba_{1-x},K_x)(Zn_{1-y},Mn_y)_2As_2$ (Fig. 3). Spectra are almost identical as temperature varies across *T*c, indicating that the electronic structure of Mn atoms maintains its high-spin state through the paramagnetic to ferromagnetic phase transition.

Typically, compression causes a tendency towards a closer packing of atoms, ions and molecules, which in turn is intimately linked to changes in electron hybridization. So application of pressure can induce major modifications in materials originally possessing substantial band gaps or vice versa [30, 31]. By undertaking As *K*-edge XMCD measurements [Fig. 4 (a) and (b)] we studied the pressure-induced magnetic instabilities of a hole under-doped sample (G1: x = 0.15, y = 0.15) and compared it with a previously studied optimally hole doped sample (G3: x = 0.25, y = 0.05) [12]. While pressure was expected to mimic the effect of doping in bringing about increased *p-d* hybridization and enhanced ferromagnetic interactions with reduction of

inter-atomic distances, this is not observed. The monotonic reduction in XMCD intensity with pressure on both samples indicates weakening of ferromagnetic interactions. Both compounds show a gradual suppression of magnetic order with pressure. The response of transport properties to pressure in the G1 sample is similar to that of the previously studied G3 sample [12], with the observation of a clear semiconductor to metal transition that is accompanied with the loss of magnetic order [Fig. 4 (c) and (d)]. This is in contrast with the proto-typical III-V DMS materials (In,Mn)Sb [32, 33] and (Ga,Mn)As [33], where *T*c increases with increasing hydrostatic pressure for samples with high concentration of band holes. Understanding the origin of the disparate response of magnetism to pressure in III-V and II-II-V DMS materials requires not only probing As *p* and Mn *d* electronic states but also the evolution of crystal structure under pressure, as discussed below.

In order to probe the electronic properties of the Mn ions under pressure, we have conducted Mn Kβ XES measurements on the optimally hole doped sample (G3: $x = 0.25$, $y = 0.05$) [Fig. 5]. The Kβ spectra for Mn were fitted using three Gaussian functions representing the Kβ', Kβ_x and K$\beta_{1,3}$ peaks, and a linear background was subtracted [25]. Derived parameters of $\Delta E'$ and I-Kβ' (Kβ' peak intensity relative to the total intensity of the main Kβ region) are displayed in the insets of Figure 5. We observe no changes outside the experimental error in electronic state under low pressure (< 10 GPa), and only a small reduction in $\Delta E'$ and I-Kβ' is detected at higher pressure (30 GPa). However, pressure suppresses ferromagnetism in the $Ba(Zn,Mn)_2As_2$ system, even at very low pressure (~ 0.5 GPa) as revealed by the As *K*-edge XMCD measurements [Fig. 4 (b)]. The exchange energy for a system of interacting atomic moments is illustrated by the effective classical Heisenberg Halmilton $H = -\sum_{i \neq j} J_{ij} \overrightarrow{S_i} \cdot \overrightarrow{S_j}$, where J_{ij} is the exchange interaction between i- and j-site local spins. Since Mn atoms maintain robust local spin state even at 30 GPa, our XES data rules out the possibility that the suppression of magnetic order arises from the collapse or suppression of Mn local spin moments. Upon hole doping, changes in *p-d* hybridization could be clearly detected in the Mn Kβ XES spectra at ambient pressure [Fig. 2 (a)], indicating that chemical doping enhances *p-d* hybridization. Under applied pressure, no obvious changes are seen in the XES spectra. These results imply that pressure induced variations in the *p-d* hybridization are too small compared with the changes induced by chemical doping, therefore hardly detected by XES measurements. Chemical doping is a more efficient driver in enhancing the exchange interactions compared with external pressure, hence more effective in inducing robust ferromagnetic order.

We now look at the transport behavior of $(Ba_{1-x}K_x)(Zn_{0.9}Mn_{0.1})_2As_2$. At ambient pressure the electrical resistivity exhibits a small decrease with increasing carrier doping level *x,* but the semiconducting behavior remains [8]. However, a semiconductor to metal transition was observed upon compression both on hole optimally doped G3 sample and hole under doped G1 sample [Fig. 4 (c) and (d)]. This contrasts with the response of III-V based GaAs / (Ga,Mn)As semiconductors, who possess a direct bandgap at ambient conditions. Under pressure, pure GaAs undergoes a direct-to-indirect bandgap transition at ~ 4 GPa [34]. Theoretical studies [35] show that the pressure behavior of the bandgap of (Ga,Mn)As DMS is very similar to that of pure GaAs with a direct-to-indirect bandgap transition at ~ 6 GPa. The bandgaps for GaAs and (Ga,Mn)As are respectively 1.7 eV at 16 Gpa and 1.3 eV at 15 GPa, showing robust semiconducting behavior even at these high pressures. The response of transport properties to pressure in $(Ba_{1-x}K_x)(Zn_{1-y}Mn_y)_2As_2$ is drastically different, with the observation of a clear semiconductor to metal transition that is accompanied by loss of magnetic order [Fig. 4 (c) and (d)]. We note that typical band gaps in the II-II-V materials study here are significantly smaller than those of the GaAs-based materials, with indirect gap of order ~ 0.2 eV [13].

High pressure powder XRD data were analyzed with Rietveld refinements using the GSAS program packages [36]. Figure 6 (a) shows the XRD patterns together with refinements at selected pressures. The averaged fitted residuals R_p and R_{wp} are 1.14% and 1.58%, respectively. Figure 6 (b) illustrates the pressure dependence of the unit cell parameters based on the Rietveld refinements. Up to a pressure of 25 GPa, the basal lattice parameter *a* contracts by 6.9 %, whereas the lattice parameter *c* drops by 11.0 %, exhibiting

obvious anisotropic compression. When applying pressure, the interlayer spacing between ferromagnetic [(Zn/Mn)As] layers (*c* axis) decreases at a much larger rate than the intra-layer $MnAs_4$ ligands (*a* axis) (crystal structure shown in left corner inset of Fig. 6 (b)). Pressure induced semiconductor to metal transition in the II-II-V based $Ba(Zn,Mn)_2As_2$ is connected to As-As hybridization [12], which is related to the interlayer As-As distance, *d*. In the compound β-$BaZn_2As_2$ [37], strong As-As hybridization as a result of a relatively short d = 3.7 Å between adjacent [Zn,As] layers leads to a secondary splitting of the bonding and antibonding states of As 4*p* levels. The latter, formed by As $4p_z$ states are found near the valence band maximum (VBM). It is shown [37] that the size of the bandgap is controlled by the proximity of these states to the Fermi level, which strongly depends on the As-As spacing. With a slight decrease in *d*, the hybridization of As atoms becomes larger, and widens the VB. As a result, the energy states at the VBM are raised and bandgap is reduced. Inset of Figure 6 (b) (besides the crystal structure) shows the changes in interlayer As-As distance *d* in the representative G4 (x = 0.2, y = 0.05) compound as a function of pressure. Upon compression, *d* gradually decreases which enhances the interlayer As hybridization (raising the energy of As $4p_z$ antibonding states), leading to a strong response of As 4*p* states to pressure. A gradual decrease in *d* in turn results in a decrease of bandgap and a semiconductor to metal transition [Fig. 4 (c) and (d)]. The As 4*p* state is delocalized because of pressure-induced enhanced hybridization between interlayer As atoms and related increase in bandwidths, as shown by XAS white-line broadening in As *K*-edge XAS measurements [see the right corner inset of Fig. 5, taken from Ref.12]. The interlayer As-As hybridization competes with the effective *p-d* hybridization within $MnAs_4$ tetrahedra, a necessary condition for enhanced exchange interactions. It is noteworthy that, hole carriers mediating the long-range magnetic ordering through *p-d* hybridization are resident on the *p* states of As, and the polarization strength of hole carries (As 4*p* states) scales with the sample magnetization [12]. Therefore, delocalization of hole carriers is enhanced under pressure, suppressing the exchange interactions between magnetic dopants.

The effectiveness of As 4*p* and Mn 3*d* hybridization in promoting stronger exchange interactions (*T*c) is also connected to changes in the local geometry of $MnAs_4$ tetrahedral units. The As-Mn-As bond angle (α angle bisected by the *c* axis) of the $MnAs_4$ tetrahedra as a function of pressure is presented in the upper right corner inset of Figure 6 (b). Structural analysis shows that the behavior of the bond angle α with pressure is attributed to the anisotropic compression of $MnAs_4$ tetrahedron. With increasing pressure, compression in the basal plane of $MnAs_4$ units is greater than that along the *c* axis, resulting in a decrease in the As-Mn-As bond angle α. This in turn reduces the overlap of As and Mn planar orbitals, decreasing effective *p-d* hybridization. Note that reduction of Mn-As bond distance with applied pressure can enhance the As 4*p* and Mn 3*d* orbital overlap as a result of band broadening [38, 39]. This will enhance *p-d* hybridization within the $MnAs_4$ tetrahedron. However, the decrease in interlayer As-As distance *d* and As-Mn-As bond angle α (insets of Fig. 6 (b)) with pressure acts to reduce *p-d* hybridization. These competing effects lead to the absence of sizable increases in *p-d* hybridization, which may account for the fact that no obvious changes have been detected in the high pressure Mn Kβ XES spectra. On the other hand, smaller *d* value broadens As 4*p* band states and results in increased carrier mobility (delocalization of mediating carriers), another essential ingredient for tuning exchange interactions and bandgap in $(Ba_{1-x}K_x)(Zn_{1-y}Mn_y)_2As_2$ [12], leading to gap closure and concomitant destruction of ferromagnetic order. Taken together, these results provide much needed microscopic insight into the origin of pressure-induced monotonic suppression of magnetism and gap closure in $(Ba_{1-x}K_x)(Zn_{1-y}Mn_y)_2As_2$ and imply that the changes in crystal structure (interlayer As-As distance and distortion of $MnAs_4$ units) play a key role in the vanishing of magnetic order and gap closure at high pressure.

Conclusion

In summary, we have studied the effects of hole doping and pressure on the ferromagnetism and electronic properties of the II-II-V based $Ba(Zn,Mn)_2As_2$ DMS system by employing Mn Kβ XES and As *K*-edge XMCD measurements. We find that hole doping increases the *p-d* hybridization strength (electron redistribution within $MnAs_4$ ligands) at the cost of reduction in Mn local spin density, resulting in enhanced

exchange interactions between Mn dopants. Unlike doping, pressure does not appear to affect the local Mn 3*d* states much and suppresses ferromagnetism gradually in both hole optimally doped and under-doped compounds. Upon compression, the bandgap is reduced and hole carriers mediating the long-rang magnetic order become delocalized, suppressing the magnetic order. Both effects are caused by the strong response of As *p* states (band broadening) at applied pressures. We revealed that changes in the geometry of $MnAs_4$ tetrahedra and interlayer As-As distance with applied pressure are intimately connected to the evolution of electronic structure in anion *p* and cation *d* states. The strength of *p*-*d* hybridization can be readily controlled by hole doping level, and its role is as important as the carrier polarization in inducing high *T*c ferromagnetism in these and related DMS materials.

Acknowledgements

We thank Dr. Y. Ding for the helpful discussion. Work at APS was supported by the U.S. Department of Energy, Office of Science, under Contract No. DE-AC02-06CH11357. Works at IOPCAS are supported by NSF & MOST of China through Research Projects, as well as by CAS External Cooperation Program of BIC (112111KYS820150017). Works at HPSTAR are supported by the National Natural Science Foundation of China under Grant No. 51527801 and U1530402. H.K.M and W. Y. acknowledge the financial support from DOE-BES X-ray Scattering Core Program under grant number DE-FG02-99ER45775. C. A. Escanhoela Jr. is supported by FAPESP (SP-Brazil) under Contract No. 2014/26450-5. HPCAT operations are supported by DOE-NNSA under Award No. DE-NA0001974 and DOE-BES under Award No. DE-FG02-99ER45775, with partial instrumentation funding by NSF.

Reference

[1] H. Ohno, A. Shen, F. Matsukura, A. Oiwa, A. Endo, S. Katsumoto, and Y. Iye, Appl. Phys. Lett. **69**, 363 (1996).

[2] H. Ohno, Science **281**, 951 (1998).

[3] I. Zutic, J. Fabian, and D. Sarma, Rev. Mod. Phys. **76**. 323 (2004).

[4] M. Sawicki, D. Chiba, A. Korbecka, Y. Nishitani, J. A. Majewski, F. Matsukura, T. Dietl, and H. Ohno, Nat. Phys. **6**, 22 (2010)

[5] T. Dietl, Nat. Mater. **9**, 965 (2010).

[6] T. Dietl, and H. Ohno, Rev. Mod. Phys. **86**, 187 (2014).

[7] M. Dobrowolska, K. Tivakornsasithorn, X. Liu, J. Furdyna, M. Berciu, K. M. Yu, and W. Waluliewicz, Nat. Mater. **11**,

444 (2012).

[8] K. Zhao, Z. Deng, X. C. Wang, W. Han, J. L. Zhu, X. Li, Q. Q. Liu, R. C. Yu, T. Goko, B. Frandsen, L. Liu, F. Ning, Y. J. Uemura, H. Dabkowska, G. M. Luke, H. Luetkens, E. Morenzoni, S. R. Dunsiger, A. Senyshyn, P. Bo ni, and C. Q. Jin, Nat. Commun. **4**, 1442 (2013).

[9] K. Zhao, B. Chen, G. Q. Zhao, X. Li, Z. Yuan, Z. Deng, Q. Q. Liu, and C. Q. Jin, Chin. Sci. Bull. **59**, 2524 (2014).

[10] A. Hirohata, H. Sukegawa, H. Yanagihara, I. Zutic, T. Seki, S. Mizukami, and R. Swaminathan, IEEE Trans. Magn. **51**(10), 1 (2015).

[11] M. Rotter, M. Tegel, and D. Johrendt, Phys. Rev. Lett. **101**, 107006 (2008).

[12] F. Sun, N. N. Li, B. J. Chen, Y. T. Jia, L. J. Zhang, W. M. Li, G. Q. Zhao, L. Y. Xing, G. Fabbris, Y. G. Wang, Z. Deng, Y. J. Uemura, H. K. Mao, D. Haskel, W. G. Yang, and C. Q. Jin, Phys. Rev. B **93**, 224403 (2016).

[13] J. K. Glasbrenner, I. Žutić, and I. I. Mazin, Phys. Rev. B **90**, 140403(R) (2014).

[14] G. sankar, P. R. Sarode and C. N. R. Rao, Chem. Rev. **76**, 435 (1983).

[15] P. Glatzel and U. Bergmann, Coord. Chem. Rev. **249**, 65 (2005).

[16] U. Bergmann, C. R. Horne, T. J. Collins, J. M. Workman, and S. P. Cramer, Chem. Phys. Lett. **302**, 119 (1999).

[17] T. Funk, A. Deb, S. J. George, H. Wang, S. P. Cramer, Coord. Chem. Rev. **249**, 3 (2005).

[18] Z. Deng, C. Q. Jin, Q. Q. Liu, X. C. Wang, J. L. Zhu, S. M. Feng, L. C. Chen, R. C. Yu, C. Arguello, T. Goko, F. Ning, J. Zhang, Y. Wang, A. A. Aczel, T. Munsie, T. J. Williams, G. M. Luke, T. Kakeshita, S. Uchida, W. Higemoto, T. U. Ito, B. Gu, S. Maekawa, G. D. Morris, and Y. J. Uemura, Nat. Commun. **2**, 422 (2011).

[19] G. Peng, F. M. F. Degroot, K. Hämäläinen, J. A. Moore, X. Wang, M. M. Grush, J. B. Hastings, D. P. Siddons, W. H. Armstrong, O. C. Mullins, and S. P. Cramer, J. Am. Chem. Soc. **116**, 2914 (1994).

[20] P. Glatzel, U. Bergmann, F. M. F. de Groot, and S. P. Cramer, Phys. Rev. B **64**, 045109 (2001).

[21] S. D. Gamblin, and D.S. Urch, J. Electron. Spectrosc. Relat. Phenom. **113**, 179 (2001).

[22] Z. Mao, J. Lin, J. Yang, J. Wu, H. C. Watson, Y. Xiao, P. Chow, and J. Zhao, Am. Mineral. **99**, 415 (2014).

[23] G. Vanko´, T. Neisius, G. Molnar, F. Renz, S. Karpati, A. Shukla, and F. M. F. de Groot, J. Phys. Chem. B **110**, 11647 (2006).

[24] K. Tsutsumi, H. Nakamori, and K. Ichikawa, Phys. Rev. B **13**, 929 (1976).

[25] S. Limandri, S. Ceppi, G. Tirao, G. Stutz, C. G. Sánchez, and J. A. Riveros, Chem. Phys. **367**, 93 (2010).

[26] B. Ravel, and M. Newville, J. Synchrotron Radiat. **12**, 537 (2005).

[27] B. T. Thole, P. Carra, F. Sette, and G. van der Laan, Phys.Rev. Lett. **68**, 1943 (1992).

[28] P. Carra, B. T. Thole, M. Altarelli, and X. D. Wang, Phys. Rev. Lett. **70**, 694 (1993).

[29] G. Y. Guo, J. Phys.: Condens. Matter **8**, 747 (1996).

[30] E. V. Zarochentsev, and E. P. Troitskaya, Phys. Solid State **44**, 1370 (2002).

[31] A. K. McMahan, and R. C. Alberts, Phys. Rev. Lett. **49**, 1198 (1982).

[32] M. Csontos, G. Mihaly, B. Janko, T. Wojtowicz, X. Liu, and J. K. Furdyna, Nat. Mater. **4**, 447 (2005).

[33] M. Csontos, G. Mihaly, B. Janko, T. Wojtowicz, W. L. Lim, X. Liu, and J. K. Furdyna, Phys. Status Solidi C **1**, 3571 (2004).

[34] P. Grivickas, M. D. McCluskey, and Y. M. Gupta, Phys. Rev. B **80**, 073201 (2009).

[35] N. G. Szwacki, J. A. Majewski, and T. Dietl, Phys. Rev. B **91**, 184409 (2015).

[36] A. C. Larson and R. B. V. Dreele, Los Alamos National Laboratory Report No. LAUR 86, 2004.

[37] Z. W. Xiao, H. Hiramatsu, S. Ueda, Y. Toda, F. Y. Ran, J. G. Guo, H. C. Lei, S. Matsuishi, H. Hosono, and T. Kamiya, J. Am. Chem. Soc. **136**, 14959 (2014).

[38] T. Dietl, H. Ohno, F. Matsukura, Phys. Rev. B **63**, 195205 (2001).

[39] Y. C. Tseng, D. Paudyal, Ya. Mudryk, V. K. Pecharsky, K. A. Gschneidner, Jr., and D. Haskel, Phys. Rev. B **88**, 054428 (2013).

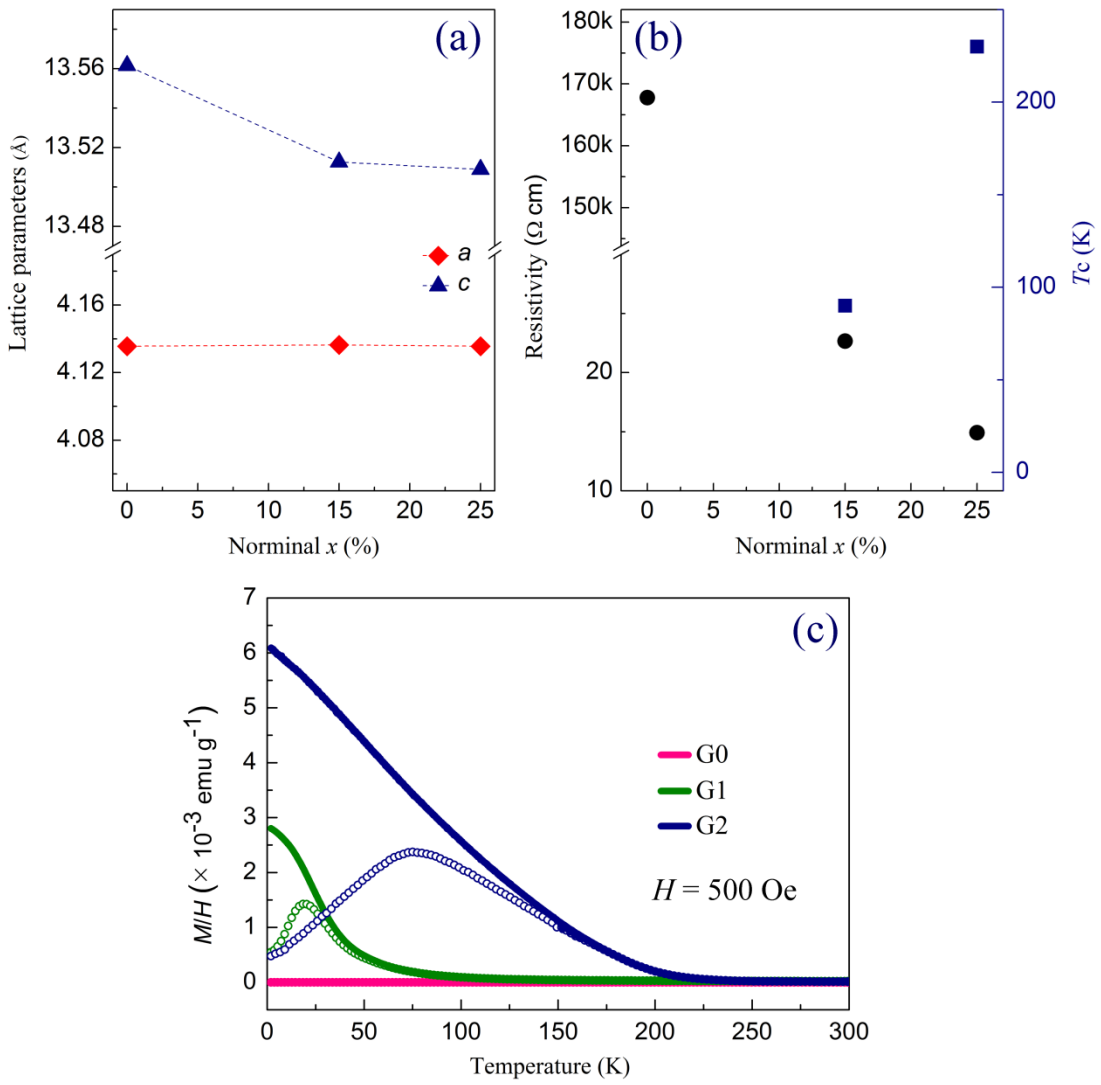

FIG.1. (a) Lattice parameters of polycrystalline samples G0, G1 and G2 $[(Ba_{1-x}K_x)(Zn_{0.85}Mn_{0.15})_2As_2$ with x = 0, 0.15, 0.25, respectively)] at ambient pressure and room temperature. (b) Low temperature resistivity (T = 20 K, black circles) for G0, G1 and G2 samples and Curie temperature Tc (blue squares) for G1 and G2 samples. (c) DC magnetization data for G0, G1 and G2 samples measured in H = 500 Oe on warming after field-cooling (solid lines) and zero-field-cooling (dotted lines).

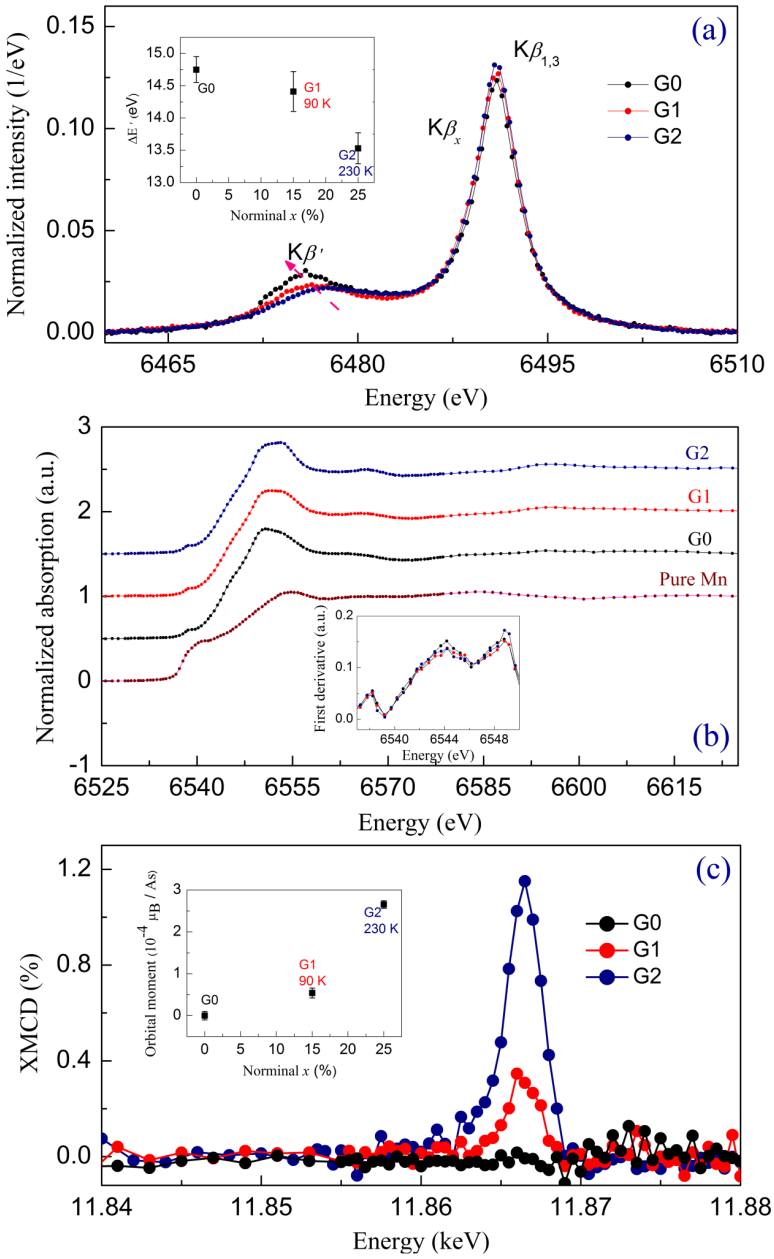

FIG.2. (a) X-ray emission Mn K β spectra of polycrystalline samples $(Ba_{1-x}K_x)(Zn_{0.15}Mn_{0.85})_2As_2$ at ambient pressure and room temperature. Compounds of different K (hole) doping level x at fixed Mn (spin) concentration y = 0.15 are defined as G0 : (x = 0, y = 0.15); G1 : (x = 0.15, y = 0.15); G2 : (x = 0.25, y = 0.15). XES spectra have been normalized to unit integrated area and then aligned around the K $\beta_{1,3}$ main peak of the G0 spectrum. Inset: the energy difference $\Delta E'$ between the K β' satellite and the K $\beta_{1,3}$ main line as a functin of x. The dashed arrow in pink is a guide to the eye. (b) Normalized XAS spectra at the Mn K-edge for G0, G1, G2 and pure Mn at T = 300K, P = 1bar. The spectra were offset in the vertical direction for clarity. Inset: the first derivative of the XAS data in the 6537- 6550 eV range. (c) As K-edge XMCD spectra for G0, G1 and G2 samples at T = 2 K, P = 1 bar. Inset: the orbital magnetic moment per As as a function of x. Values of Curie temperatures are included in the insets next to each compound label.

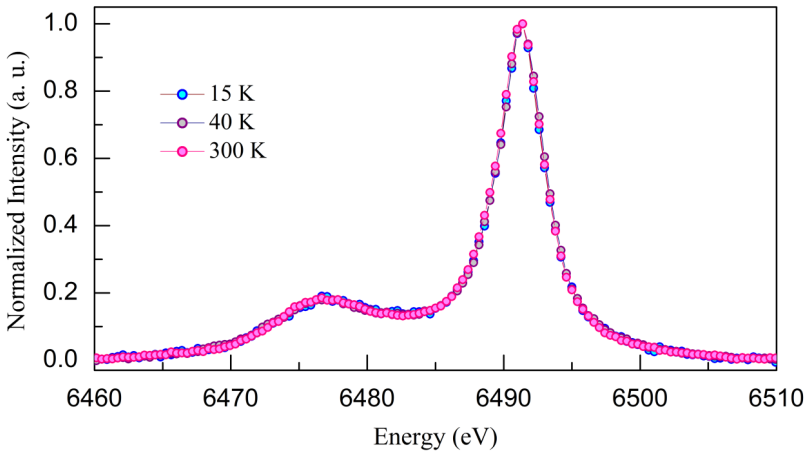

FIG. 3. XES spectra of polycrystalline $(Ba_{1-x}K_x)(Zn_{1-y}Mn_y)_2As_2$ (x = 0.15, y = 0.15, Tc = 90 K) at different temperatures and ambient pressure. The intensities of the plots were normalized to the K $\beta_{1,3}$ maximum.

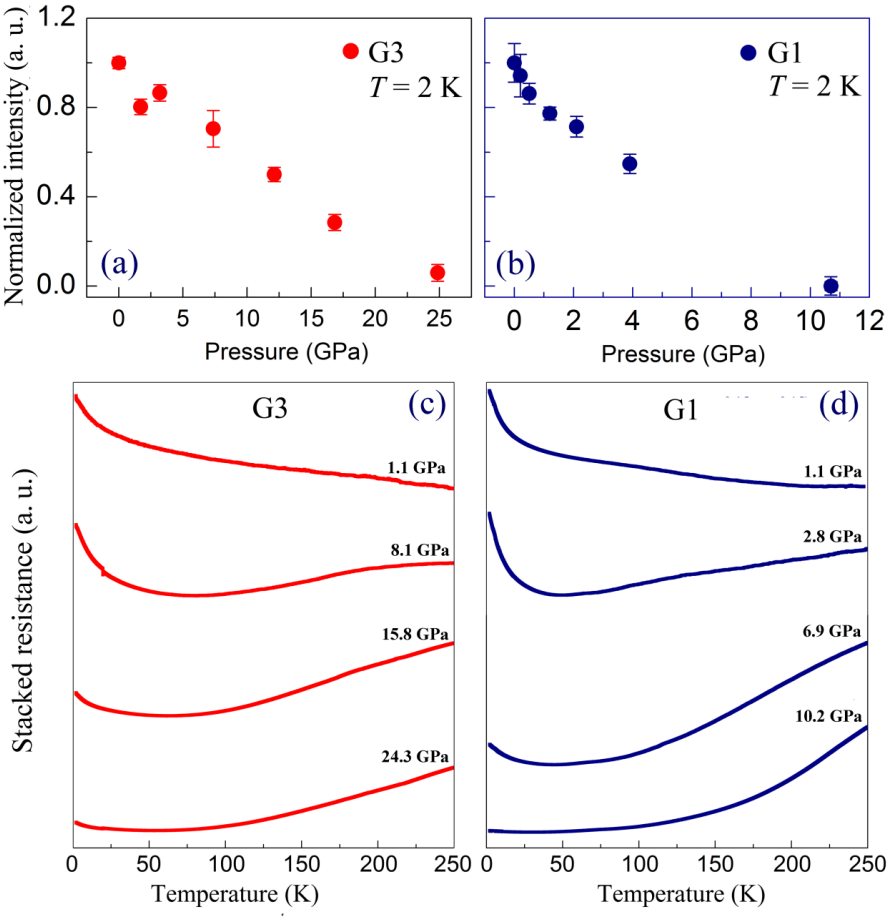

FIG. 4. Pressure-dependent As K-edge XMCD peak intensity for polycrystalline $(Ba_{1-x}K_x)(Zn_{1-y}Mn_y)_2As_2$ at 2 K: (a) G3: (x = 0.25, y = 0.05). (b) G1: (x = 0.15, y = 0.15). The XMCD peak intensities of both samples were normalized to unity at P = 1 bar. Temperature dependent resistance plots at selected pressures for the same samples. The As K-edge XMCD and transport data of G3 sample was taken from Ref. 12.

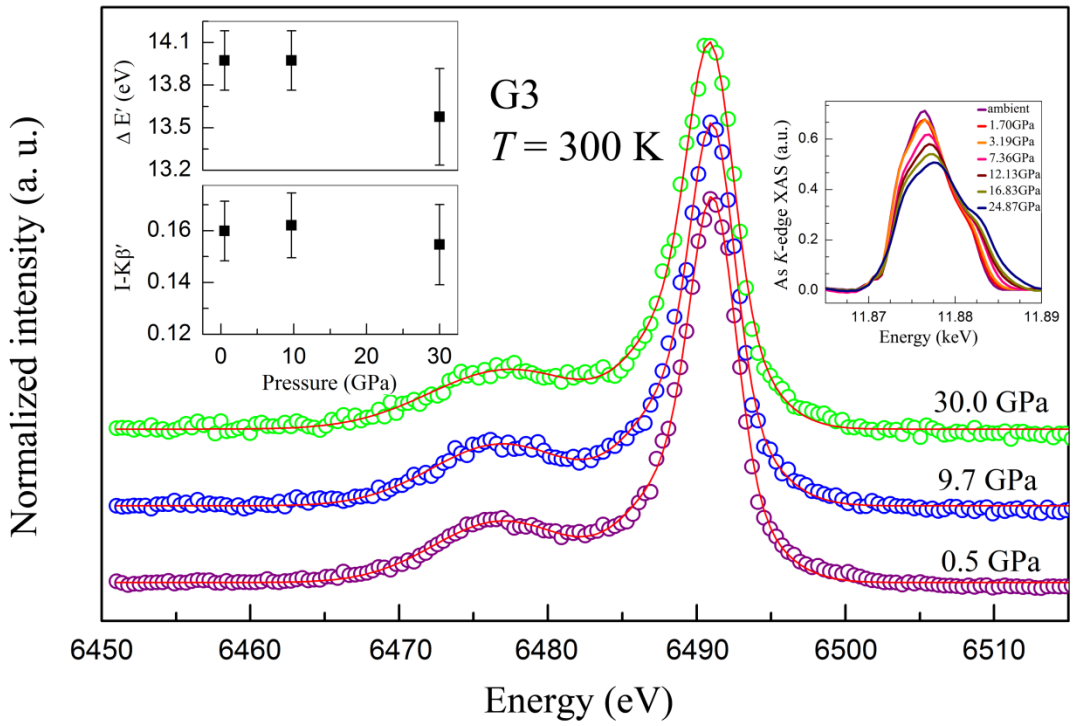

FIG. 5. X-ray emission spectra of polycrystalline G3: (x = 0.25, y = 0.05) at high pressures and room temperature. The spectra were shifted in the vertical for clarity. Red solid lines are fits using three Gaussian functions as described in the text. Left corner inset: energy difference $\Delta E'$ and line intensity I- Kβ as a function of pressure. Right corner inset: background-subtracted "white line" peaks in As K-edge XAS spectra under different pressures for G3 sample, taken from Ref. 12.

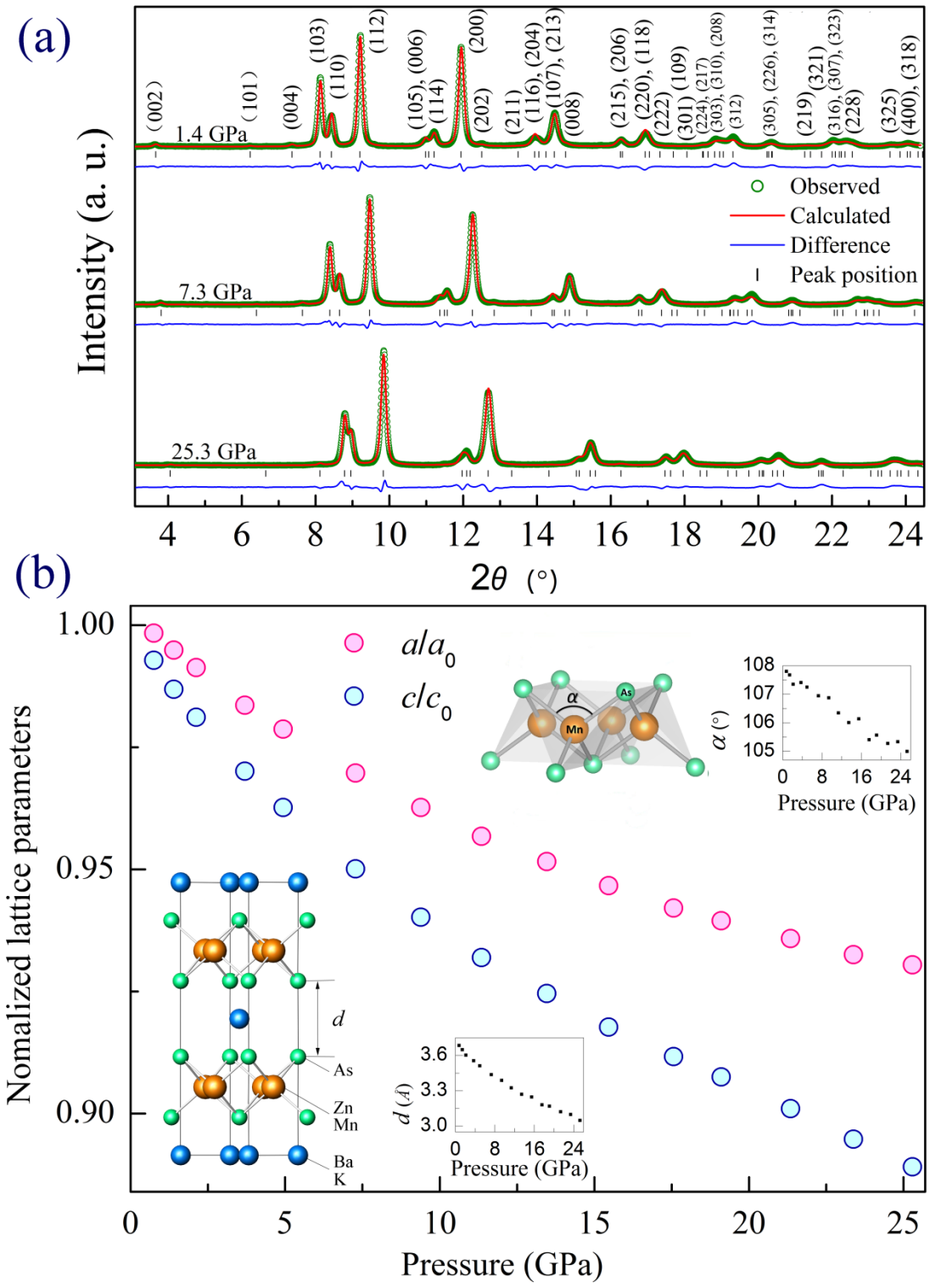

FIG. 6. (a) XRD patterns of polycrystalline $(Ba_{1-x}K_x)(Zn_{1-y}Mn_y)_2As_2$ G4: (x = 0.20, y = 0.05) at selected pressures and room temperature. The XRD patterns are refined using Rietveld Method. (b) Lattice parameters as a function of pressure. Data were normalized to unity at P = 1 bar. Left corner inset: crystal structure of $(Ba,K)(Zn,Mn)_2As_2$ belonging to tetragonal $ThCr_2Si_2$ structure, and the pressure dependence of interlayer As-As distance d. Upper right corner inset: $MnAs_4$ tetrahedron geometry, and the pressure dependence of As-Mn-As bond angle α (bisected by c axis) in the $MnAs_4$ tetrahedron.